Drill-bit signal

Clement Kostov

ABSTRACT

The goal of the "VSP while-drilling" project is to obtain images of the subsurface from the drill-bit signal recorded with a seismic array at the surface. The signal-processing techniques developed in the course of this project are aimed at detecting a weak non-impulsive source among several sources of coherent noise. These techniques could also be of interest for conventional surface seismic processing.

Spectral analysis of field data shows evidence of a weak signal from the drill-bit. I suggest alternatives in the acquisition of the data, and discuss models for the signal that could enhance the processing.

INTRODUCTION

The "VSP while drilling" experiment consists of recording seismograms with an array at the surface during the drilling of a well. The goal of the project is to obtain images of the subsurface comparable to images from surface seismic or VSP experiments.

The raw records of "VSP while-drilling" data are similar to uncorrelated Vibroseis data where the source is also non-impulsive (Kostov and Zanzi, 1988). Further challenges for the processing of "VSP while-drilling" data are the presence of several sources at the surface that are strong compared to the downhole source, as well as the lack of a time-origin and a record of the source wavelet.

Since the last report, I have worked with part of the data acquired by the *Osservatorio Geofisico Sperimentale* (OGS) during a large-scale experiment to record drill-bit signal (Progetto Geobit, 1988). The experiment was aimed at recording not only the acoustic waves in the far-field of the borehole, but also the sources of noise and the drill-bit wavelet (source signature). These additional measurements were done with geophones on the drilling platform and accelerometers on the drilling rig.

Still, the processing of these data shows that, although detectable, the signal from the drill-bit is very weak.

What can be done – both in acquisition and processing – to amplify the drill-bit signal?

The acquisition of the data includes: (1) familiar elements, such as the design of the surface seismic array to sample correctly both the signal from the sources at depth and from the strong surface sources, (2) possibilities for breakthroughs by clever recording of the drill-bit signal and the sources of noise, and (3) understanding the dependence of the drill-bit signal on the drilling conditions.

In the processing of the data from the OGS experiment, I have enhanced weak sources by summing spectra (incoherent summation) for several 10 seconds long gathers. The next step is to sum the data coherently by appropriate phase and moveout corrections. Further, the detection of a weak source could be improved if the processing takes advantage of models – point sources, or bandwith, or arrangement of spectral lines – for the sources of signal and noise.

In the first part of this report I describe the OGS experiment, comment on alternatives for the acquisition of the data, and present the results of the 2-D spectral analysis. In the second part, I discuss two models for the drill-bit signal which could lead to improved processing methods: (1) a model of a signal generated by impacts repeating at equal intervals of time, and (2) the estimation of the drill-bit wavelet assuming known the delays across the array for the direct arrivals from the drill-bit.

THE OGS EXPERIMENT

The data for the OGS experiment were recorded during the drilling of a 1.5km deep well through flat beds of sedimentary rocks, mainly sand and clay. No deviation of the well is indicated in the observer's report.

There are five types of records from that experiment – (1) surface array data, (2) accelerometers on the drilling rig, (3) geophones on the drilling platform, (4) geophones buried up to 60 m deep, and (5) standard drilling logs and stacking velocities from surface seismics. I will describe each of the five types of records and then suggest a new acquisition geometry for future experiments.

The seismic array

The parameters of the seismic array are summarized in the following table:

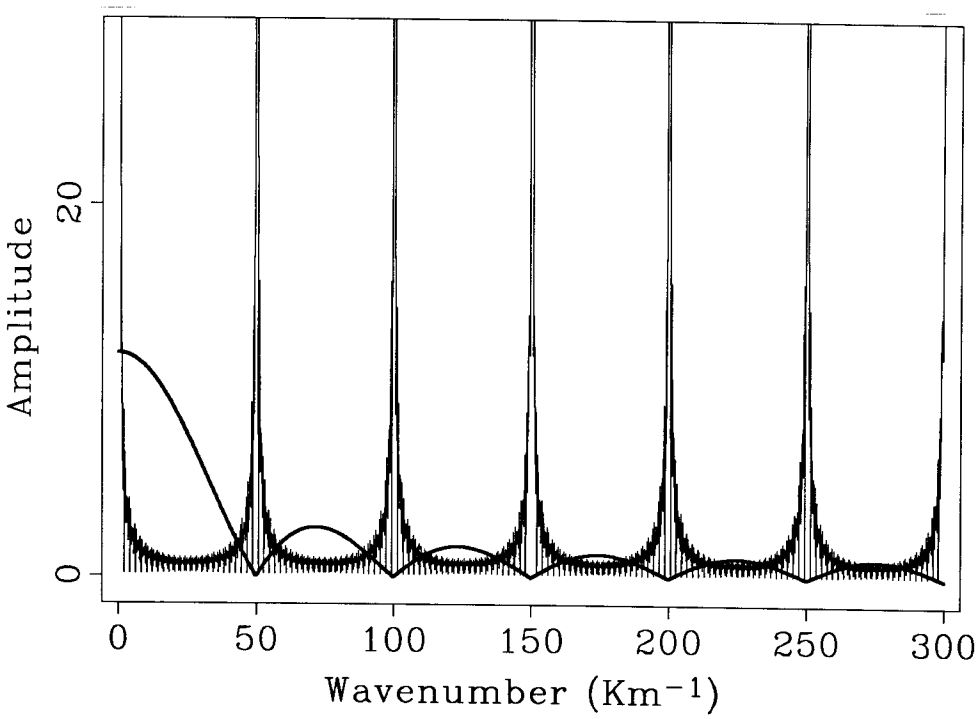

FIG. 1. Array patterns for the groups and channels used in the OGS survey. Uniform spacing of the geophones ensures that the zeros of the group pattern cancel the aliases of the channel pattern.

Array Parameters	
Offset range	0.1 to 1.5 km
Channel spacing	20 m
Number of channels	72
Groups	12 geophones per group, spaced 1.66 m apart, uniform weighting
Geophones	Vertical component, buried at 0.7 m depth

In addition, there were horizontal component geophones every 100 m. The offset range was modified when the depth of the well reached 1 km – the nearest offset became 0.385 km and the farthest offset became 2.1 km.

Figure 1 displays the group and channel array patterns for the OGS survey. The regular spacing of geophones implies that summing all channels is equivalent to summing all geophones, thus creating a long and densely sampled array for detecting waves arriving with zero-delay at the array. Figure 1 also illustrates this observation by showing that the zeros of the group array pattern cancel the peaks of the aliased channel array pattern.

The choice of the group parameters results, as usual in seismic acquisition, from a trade-off between attenuating surface-waves and retaining high frequencies of the signal. A further comment about the drill bit survey is that there might be strong surface energy unrelated to the drilling and propagating at any direction with respect to the array.

The choice of the lengths in time of the individual "shot" gathers, and of the duration of the gaps between gathers, are issues best answered from experience. In the early stages of the project it is good practice to acquire records as long as practical – 1 to 2 minutes – and to record several shots, such that the movement of the bit between "shots" is only a few meters. In general, velocity analysis, where incoherent summation is possible, will be less affected by gaps in the recording than deconvolution, where the relative phase between gathers is important. The following table summarizes the recording parameters for the OGS survey:

Recording Parameters	
Sampling rate in time	0.002 seconds
Length of records	10 or 25 seconds
"Shot spacing"	1 to 10 minutes apart, corresponding to vertical movement of the drill bit 1 to 5 m
Number of "shot" gathers	1200

For the work presented in this report, I had available 3 sequences of about 30 gathers, each gather 10 seconds long. The gathers were recorded for depths of the drill bit at about 0.4 km, 0.8 km, and 1.4 km.

Figure 2 displays the frequency spectra for the individual traces in a "shot" gather. The traces have been normalized to constant power and the amplitude of the strongest frequency component just above 18Hz has been clipped on the figure. The strongest spectral lines can be related to the spectra of the surface equipment, commented upon in Figure 4.

Accelerometers on the drilling rig

In an attempt to record the drill bit wavelet, a three-component accelerometer was installed on the drilling rig. The accelerometer had a measurement range of $\pm 5g$, and was manufactured by Schaevitz Engineering, Pennsauken, New Jersey. Due to logistic problems, records from the accelerometers were obtained only for an interval of 200m of drilling.

Accelerometers have been used with some success since the late 60's to produce "instantaneous logs while drilling", (Lutz et al., 1972). A major difficulty with measuring the signal at the top of the rig, and relating that signal to the drill bit signature, is that the propagation of waves along the borehole modifies the the signature in a complex way.

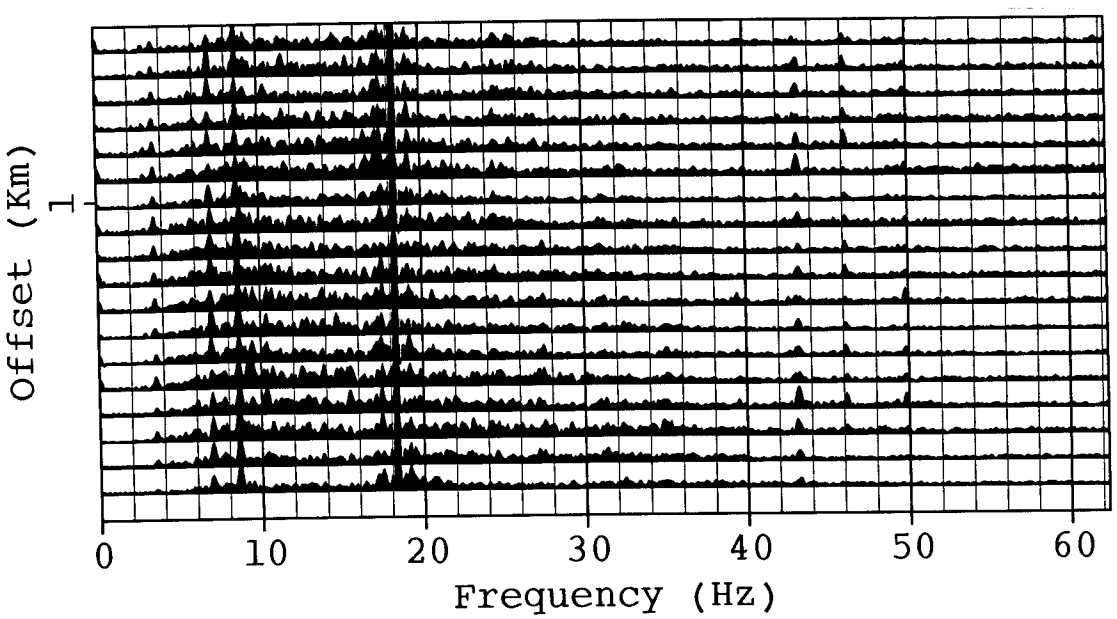

FIG. 2. Spectra of the traces of the surface array for a "shot" gather. Dominant spectral peaks correspond to surface waves.

If the accelerometer data provide indeed a model for the drill bit signal, then cross correlation between the array data and the accelerometer data should enhance that signal. I tried this method with the three accelerometer records which I had available, and did not observe the expected moveout across the array data, consistent with the depth of the drill-bit and the seismic stacking velocities. On the other hand, three records of 10 seconds each are not enough to draw conclusions about that approach.

Figure 3 shows one of the spectra for the vertical component of the accelerometer. The spectra of the accelerometers are significantly different from the spectra recorded on the surface or at depth. For instance, the 18Hz component, dominant on all other records, is relatively weak on the spectrum of Figure 3.

Geophones on the drilling platform

Noise on the drilling platform was recorded with five geophones – one vertical-component and one horizontal-component geophone near the top of the borehole, one near the trailer, another near the pumps, and a last one near the mud pits. Cables and geophones were buried 0.7m deep. The goal of recording the noise on the platform is to determine the frequencies excited by different equipment. Since the geophones were located in the near-field of sources distributed over a large area, the amplitudes of the recorded signals be affected strongly by the radiation patterns of the sources.

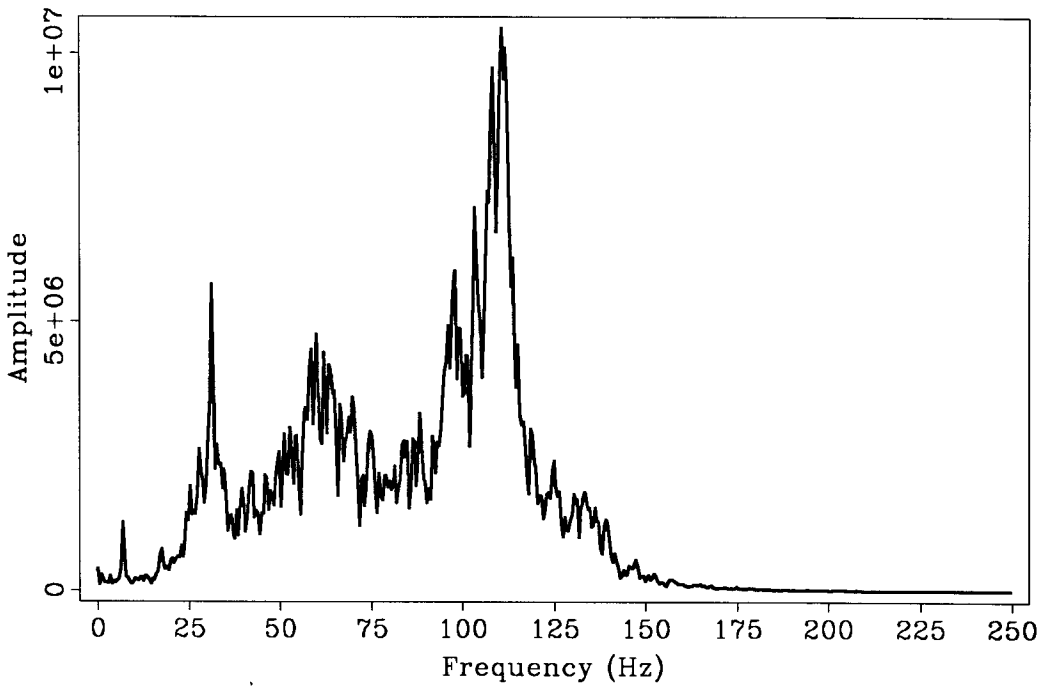

FIG. 3. Spectrum of an accelerometer record.

Figure 4 shows examples of spectra for the vertical component geophones positioned near the trailer, the pump, and the mud pit. The strong frequency near 18Hz is also the dominant frequency on the surface array data (Figure 3). This 18Hz frequency appears to have the highest amplitude relative to other frequencies on the geophone near the pump. In addition, measurements of this frequency on several "shot" gathers correlates well with the flow-rate indicated on the drilling log, which is computed by counting the frequency of the pump's piston strokes (Figure 5).

Geophones buried up to 60 m

Three, three-component geophones were buried in a shallow well at the beginning of the seismic line, at 100 m offset from the well. The depths of the geophones were 20 m, 40 m, and 60 m. The purpose of these geophones was to appreciate the attenuation of surface waves with depth (Progetto Geobit, 1988). Another possible use of deeply buried geophones would be as a vertical antenna.

Figure 6 compares the spectra of a vertical-component geophone at the surface, and a vertical component geophone at depth 60 m below the first one. The strong frequency component around 18Hz, possibly a head wave (see section on spectral analysis below), has been attenuated little relatively to other frequencies. Spectral peaks around 10Hz, corresponding to surface waves, have been significantly attenuated with respect to the background level of signal.

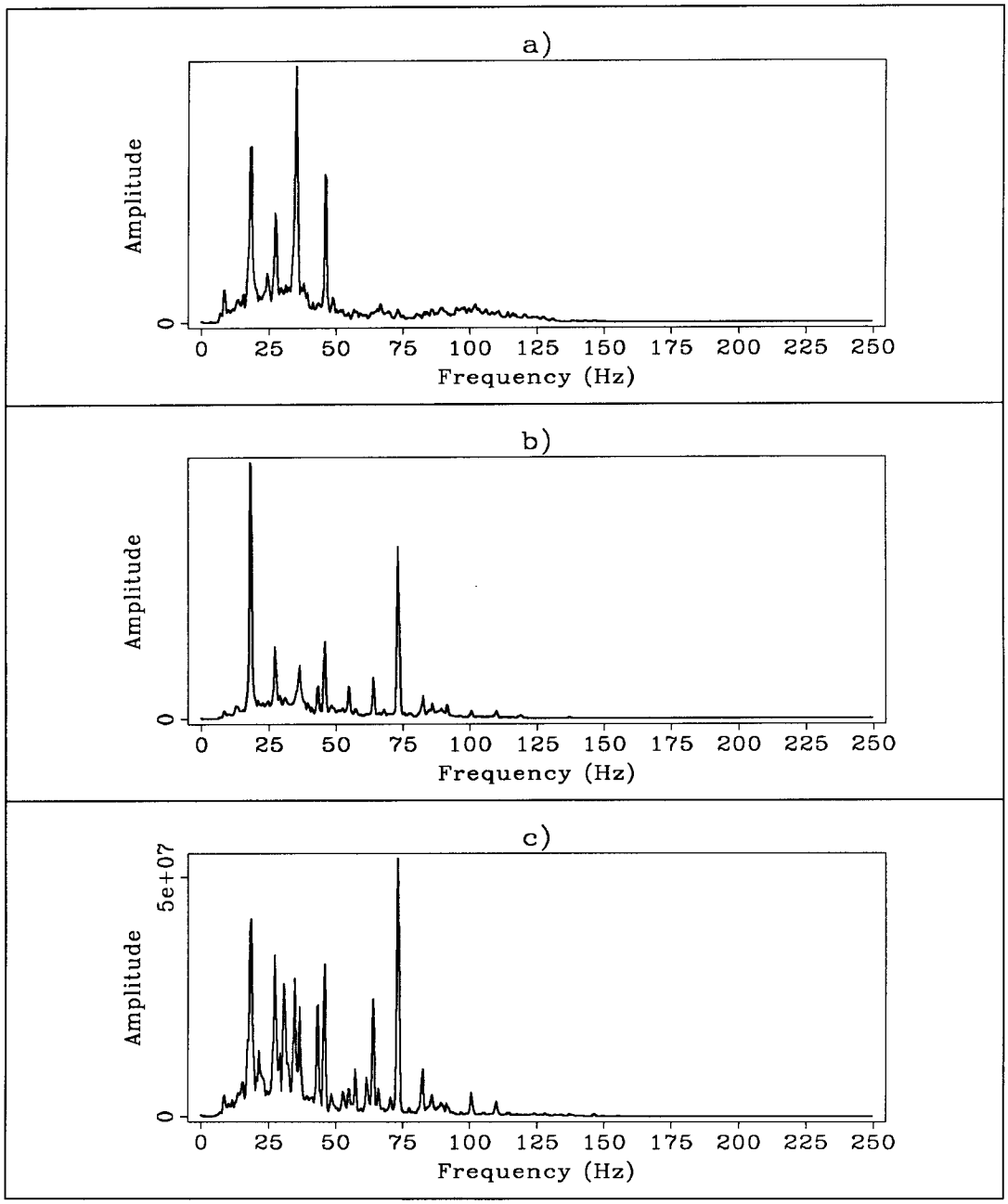

FIG. 4. a) Spectrum of the geophone near the trailer. b) Spectrum of the geophone near the pump. c) Spectrum of the geophone near the motors.

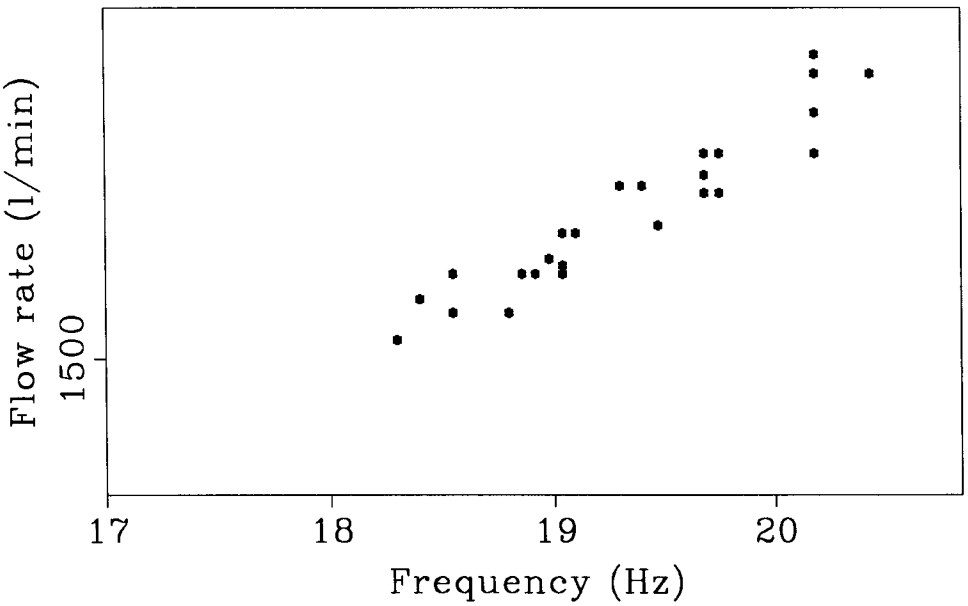

FIG. 5. Peak frequency on the seismic array gathers versus flow-rate for approximately the same time period. The strong correlation between these two variables corroborates the hypothesis that the peak frequency is related to the operation of the pump.

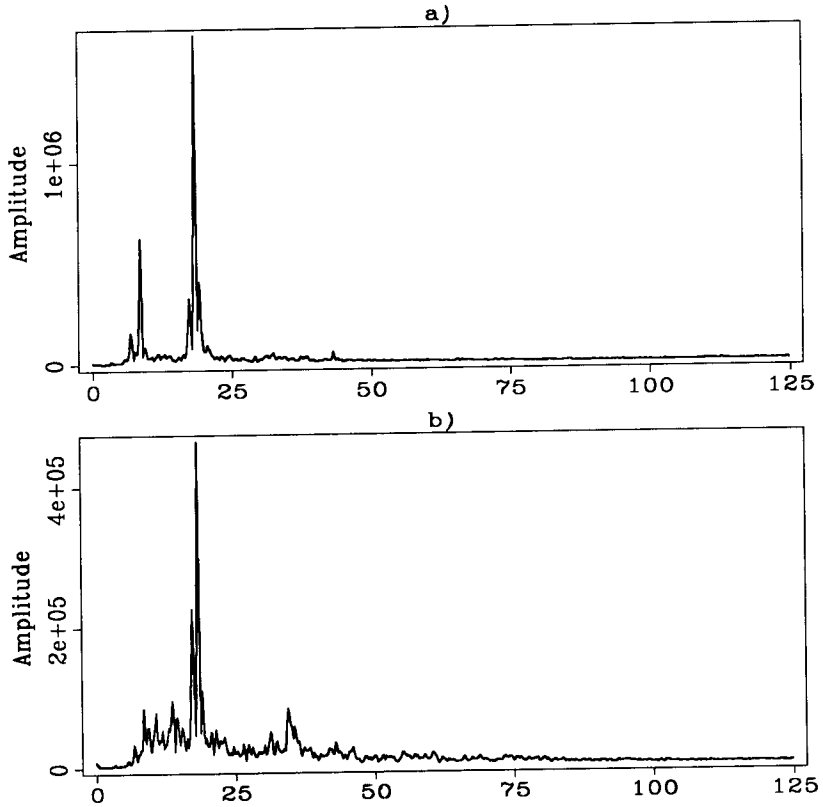

FIG. 6. Comparison of spectra for geophones a) at the surface and b) at 60 m depth.

Drilling logs

The drilling logs list several parameters at intervals of about 2-3 minutes, not necessarily related to the time when measurements are taken with the geophones. The list of parameters includes depth of the well, time of measurement, weight on bit, rotations per minute, torque, rate of penetration, flow rate, injection pressure, and volumes of mud in the pits.

The power transferred to the drilling assembly is given by the product of the torque times the rotation frequency (Lutz et al., 1972). Qualitatively one would expect strong signal from the drill bit when drilling a hard formation for which weight on bit, torque, and rotation rates are high. For the OGS survey, the formation being drilled was soft, mainly sands and clay. Extreme and typical values for some drilling parameters from the OGS survey are given in the following table:

From the drilling logs			
Parameter	min	max	typical
Weight on bit (tons)	1	8	3
Rotations per minute	30	100	70
Torque (kgm)	10	350	80
Rate of penetration (min/m)	.1	10	3

Some values for stacking velocities from surface seismic near the survey site are:

Stacking Velocities	
Time (sec)	RMSV (km/sec)
0.1	1.65
0.4	1.675
0.7	1.825
1.	1.95
1.2	2.1
1.52	2.325

Suggestions for the next acquisition of data

Figure 7 sketches my suggestion for the layout of the surface seismic lines. The new element in this acquisition geometry is the circular array at about 400m from the borehole. Energy from the drill bit will arrive with close-to-zero delay at the circular array; this should be quite independent from the velocity field provided that it is axially symmetric. Certain types of surface waves from the drilling platform will also arrive with zero delays at the circular array; attenuation of surface waves can be achieved by groups of geophones in 2-D or 1-D sub-arrays, and by filtering

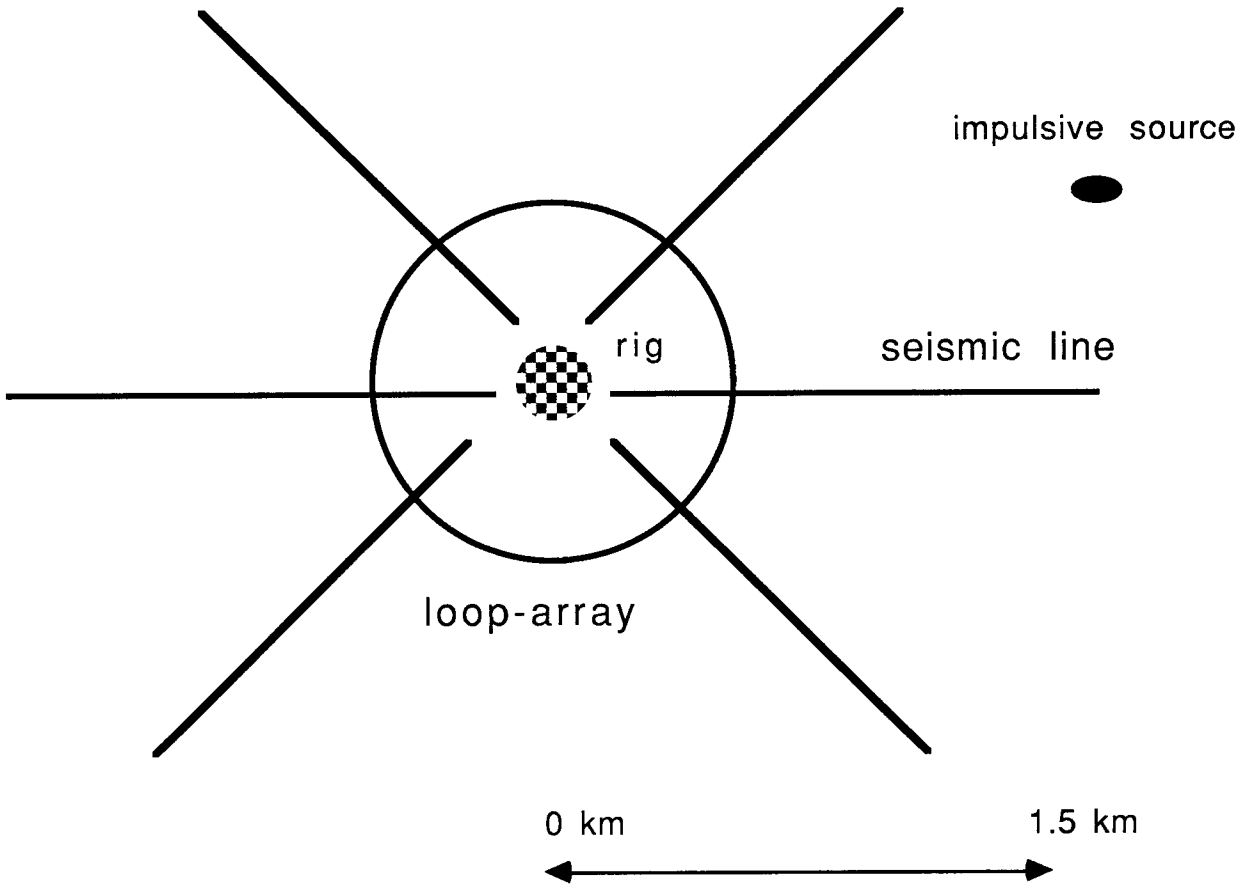

FIG. 7. Suggested acquisition geometry for a "drill bit VSP" survey. There are three split-spread seismic lines, each about 3km long, and a "loop" at a distance of about 0.4km from the well. An impulsive source could be used to obtain conventional seismic data with the same arrays in order to correct for near-surface effects.

out surface waves whose frequencies and amplitudes have been determined from the surface arrays and the geophones on the drilling platform.

The circular array will serve the same purpose as the vertical array. It will enhance the vertically propagating waves in order to obtain a model for the drill bit signal for deconvolution. The advantages of the circular array as opposed to the vertical array are easier layout, and robustness of stacking with respect to velocity. On the other hand, the use of the circular array depends on efficient attenuation of the surface waves.

In Figure 7 there are also several seismic lines on the surface. In that way, waves arriving perpendicular to the array could be separated from vertically propagating waves, signal to noise ratio would be improved, and also variations in the structure around the borehole could be imaged.

Recording of a few gathers with a conventional, impulsive seismic source, would also help to calibrate the array and the geophones on the platform for near-surface amplitude and static-delay effects. Naturally, the design of the acquisition geometry has to take into account the limited number of geophones and channels, as well as the space and time available for laying the lines.

FREQUENCY-WAVENUMBER ANALYSIS OF THE OGS DATA

A recommended implementation of the periodogram method for 1-D spectral analysis is to first split the data into overlapping segments, then apply a window function and compute the DFT in each segment, and finally average the DFT's from each segment (Marple, 1987). This method confers statistical reliability to the spectral estimates, although at the cost of some loss in resolution, since the spectrum is computed from segments of smaller lengths.

To estimate the frequency-wavenumber spectra from the array records of the OGS survey, I follow a similar method and average the spectra from 30 consecutive "shot-gathers" after applying a divergence correction along offset, and window functions in time and offset. The strongest frequency, due to the pump, is removed by applying a notch filter. The gathers correspond to positions of the drill bit between 0.79km and 0.83km. The events of interest – surface waves, direct arrivals from the drill bit, and reflections – vary from gather to gather. However, these variations, due to fluctuations in the frequencies excited by the surface equipment, or in moveout across the array, due to the increasing depth of the tool, will be small.

Figure 8 shows the average frequency-wavenumber spectrum for these 30 gathers. Notice the strong aliased energy below 15Hz. There is hardly any coherent energy above 20Hz. While the frequency-wavenumber (ω, k) spectrum is convenient to appreciate aliasing, the apparent velocity of events – equal to ω/k, is not readily determined from that plot. The transform to "ray-parameter"-frequency space is better suited for determining apparent velocities. Figure 9 shows the transform

to "ray-parameter"-frequency domain for the same data. Linear moveout to ray-parameter $p = 3$km/sec was applied before computing the spectrum. As a result of the linear moveout, the high-wavenumber events are not folded in the spectrum – there are four modes of dispersive surface waves that can be seen on Figure 9. The two hyperbolas, indicated with black dotted lines on Figure 9, correspond to wavenumbers ($k = \omega \times p$) equal to the Nyquist spatial frequency.

Next, I apply two dip-filters – one to attenuate all energy corresponding to events propagating towards the well, and another one to remove events with low apparent velocities. The first dip filter is a quarter-plane dip filter, (Dudgeon and Mersereau, 1984), and is implemented as two 1-D convolutions with a Hilbert transform. The second filter is a dip filter, which I implement in the offset-frequency (ω, x) domain, following a method described by Hale and Claerbout, 1983. Both dip-filters are implemented as zero-phase filters.

Figure 10a shows the resulting average spectrum. Some energy with apparent velocity of 1.7km/sec can be seen now for frequencies between 25 and 50Hz. Such energy could come either from the drill bit signal, or from reflections from surface sources. It is unlikely that such energy would come from aliases. A deconvolution operator, derived from the geophones near the pump and the trailer, is applied before computing the spectrum in Figure 10b. The deconvolution has diminished some of the spreading along the wavenumber axis noticeable in Figure 10a.

In Figures 10a and 10b, the result of applying a notch filter near 19Hz is seen as a black horizontal line. The peak along wavenumber for this frequency component corresponds to an apparent velocity of 1.5km/sec. As mentioned previously, this wavefield is probably generated by the pump; the velocity of propagation might then indicate a refracted wave at the water table.

To check whether the apparent velocity of these events changes when the depth of the drill bit changes, I applied the same transform to a sequence of forty gathers for depths of the drill bit between 1.4km and 1.5km. No high-velocity energy was apparent on the average of the spectra; however on few of the spectra there were such high-velocity events. Figure 11 is the average of two spectra where events with high-apparent velocity were noticeable. The apparent velocity of these events is different from the velocity of the events in Figure 10, which is an argument in favor of a deep source.

The results of this 2-D spectral analysis show that there might be signal from the drill bit, and that in any case this signal is very weak on individual 10 seconds long gathers. Coherent summation of several records should be applied to sharpen the spectra, and provide velocity information that could be used for deconvolution.

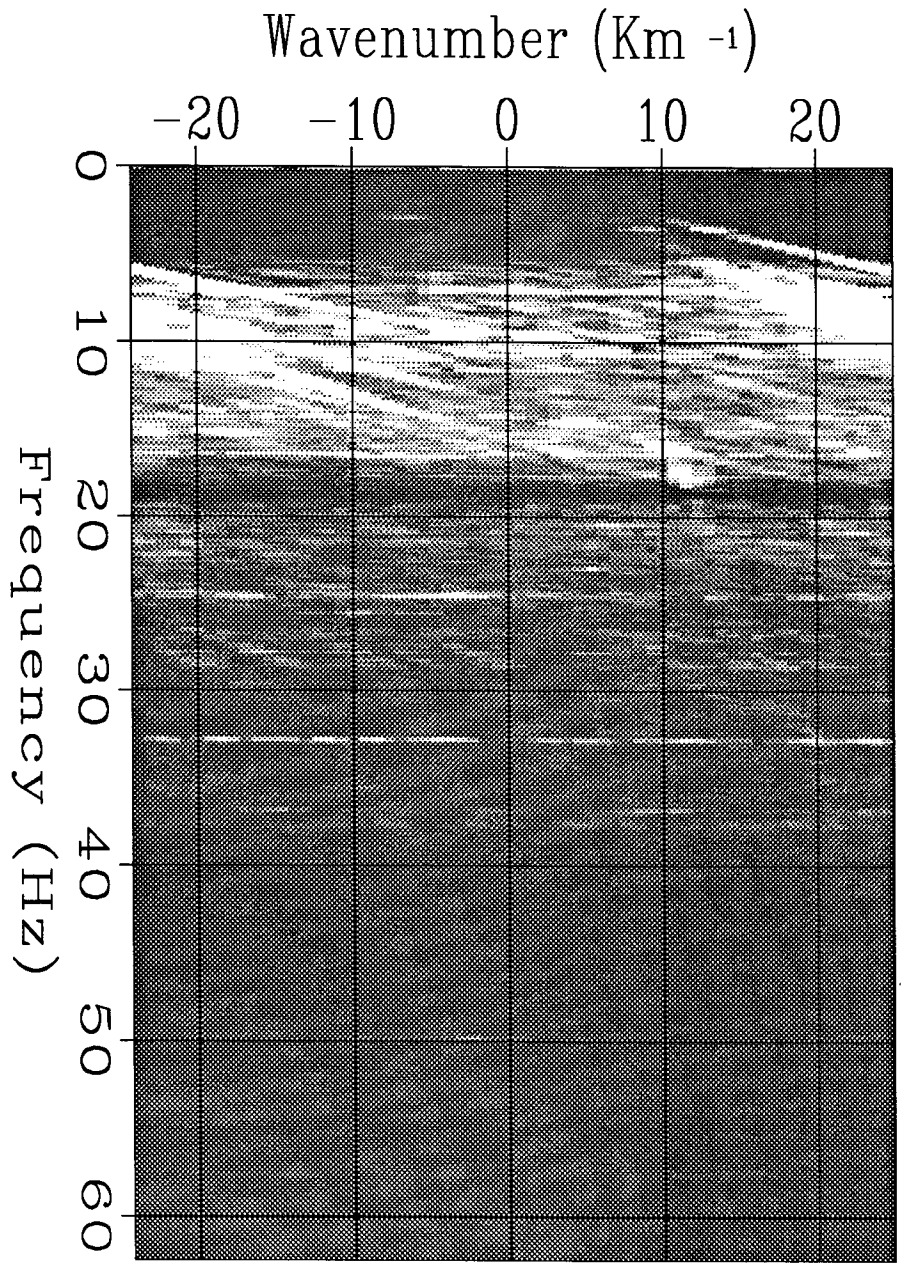

FIG. 8. Average of frequency-wavenumber spectra for 30 consecutive gathers, each 10 seconds long, corresponding to positions of the drill bit between 0.79 km and 0.83 km.

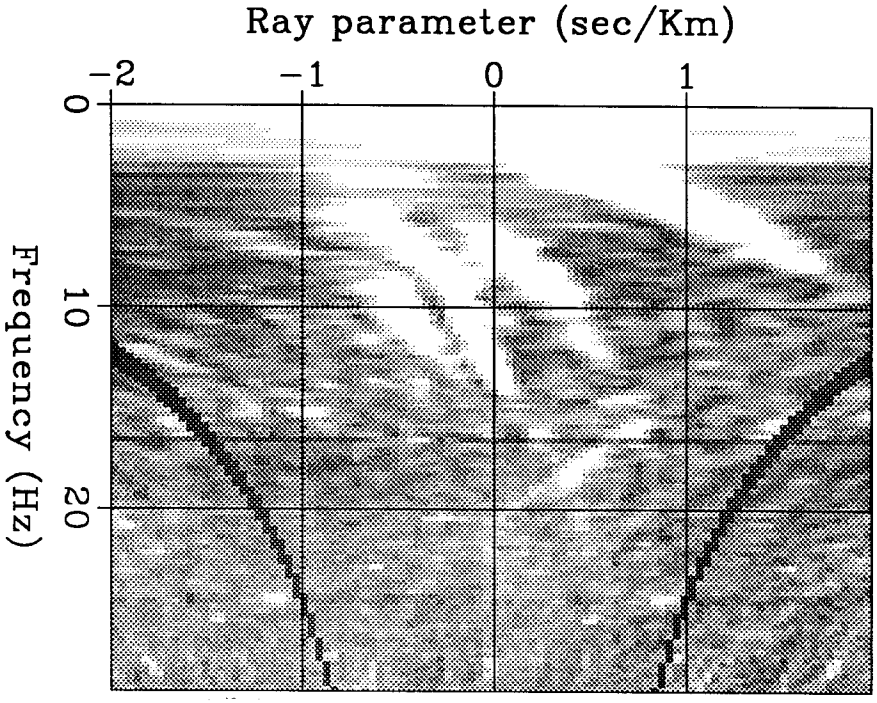

FIG. 9. Average of 30 "ray-parameter"-frequency spectra computed after applying linear moveout with ray-parameter p = 3sec/km. The surface waves are not folded on that spectrum; several dispersive modes are apparent.

A SPECULATIVE MODEL FOR THE DRILL-BIT SIGNAL

A model for the variability of the drill-bit in time – bandwidth, periodicity in time, stationarity – would be a very helpful information for the processing.

Lutz et al., 1972, argue that the signal from the drill bit is generated by percussions; as the bit-teeths lift the tool up and down, the signal is generated by a series of impulses that occur at equal intervals of time. The Fourier Transform (FT) of such a time series is a sequence of spectral lines, where the frequencies $\omega_k = k \times \omega_0$ are integer multiples of a fundamental frequency ω_0. If the amplitudes of the time sequence are modulated, the FT is convolved with the FT of the modulating function.

This plausible mechanism for the generation of the drill-bit signal raises the question of how to detect a sequence of harmonic spectral lines and how to estimate their fundamental frequency.

Estimation of the fundamental frequency of a harmonic sequence

I will introduce first a measure for the cumulative power of frequencies belonging to a harmonic sequence. Let F denote the spectrum of a time series, and H_1 the cumulative power for a harmonic sequence, with fundamental frequency ω_0 :

$$H_1(w_0) = F(w_0) + F(2w_0) + F(3w_0) + \dots . \qquad (1)$$

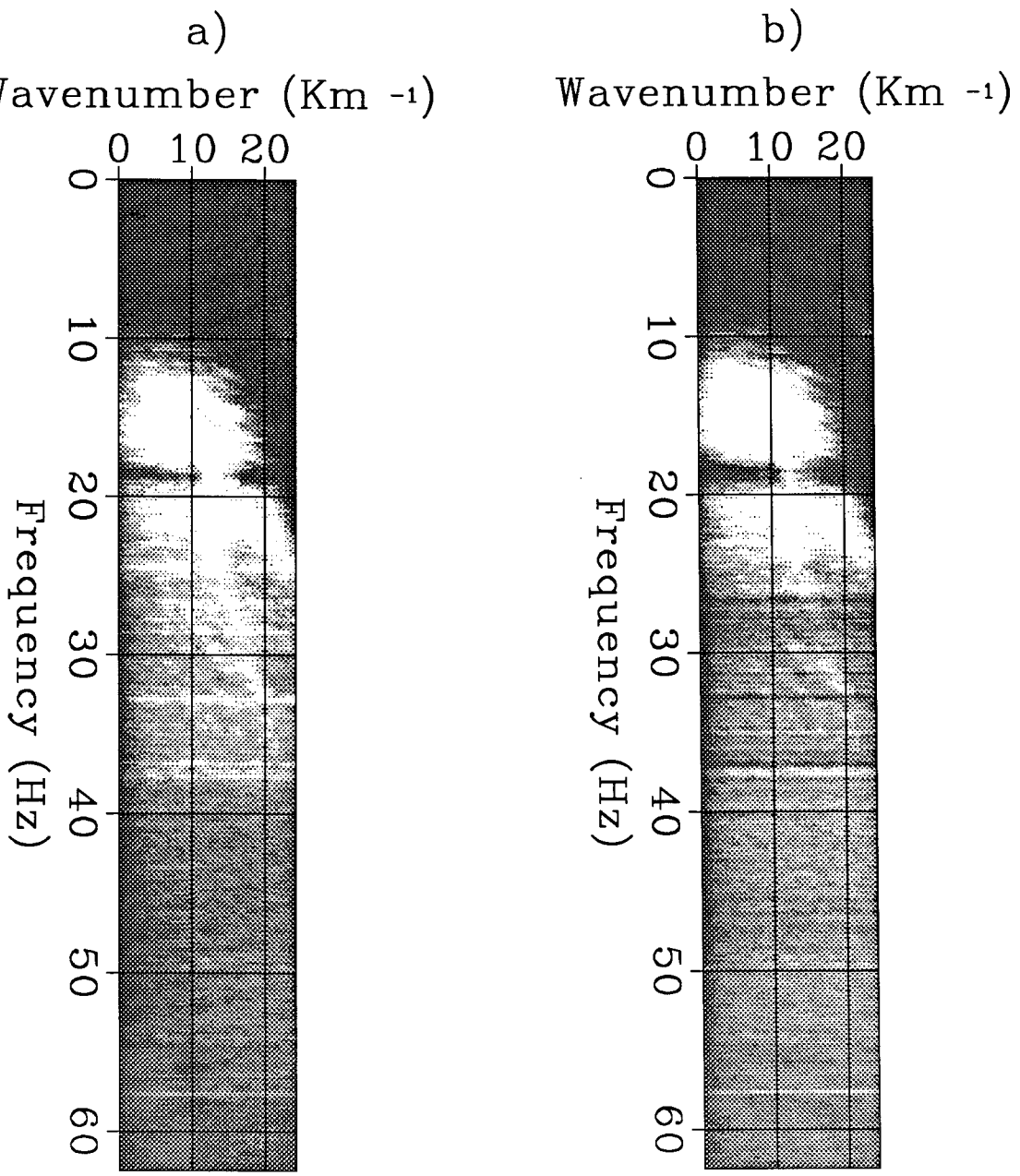

FIG. 10. Average of frequency-wavenumber spectra for 30 gathers. Dip-filters have been applied to attenuate waves traveling toward the well and waves with low apparent velocity. The events with apparent velocity of 1.7km/sec in the band between 30 and 40Hz could be drill bit signal. a) Only dip-filters are applied. b) Dip-filters and a deconvolution operator derived from the geophone near the pump are applied.

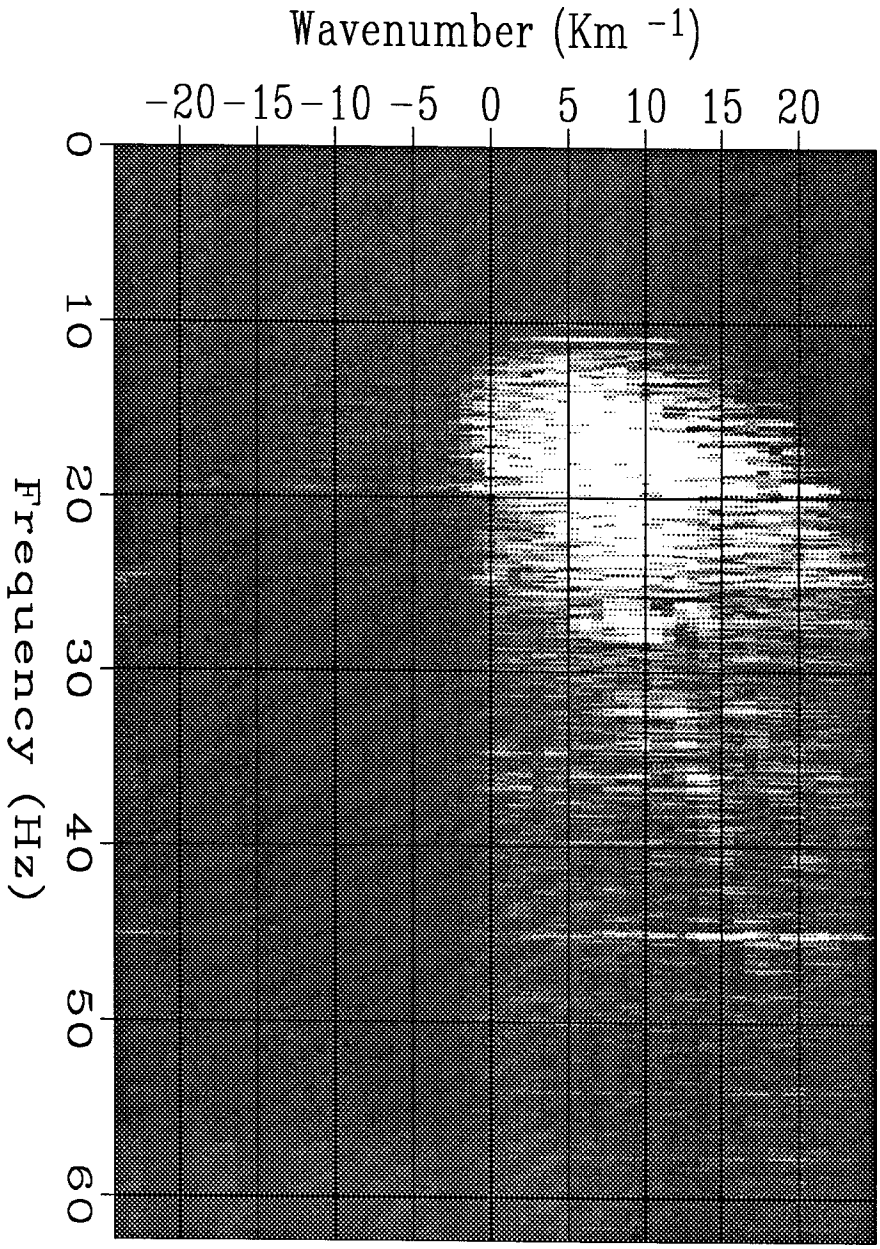

FIG. 11. Average of two frequency-wavenumber spectra for depths of the drill bit around 1.4km. The apparent velocity of the events in the frequency band 30 to 50Hz is 2.6km/sec.

The estimators of the fundamental frequencies of harmonic series will be the local maxima of the measure H_1.

Evaluating this measure by interpolation of the values of the spectrum F, computed at the grid points of the Discrete Fast Fourier Transform (DFFT), would be inaccurate, since most of the elements of the harmonic sequence will be off the grid of the DFFT.

More accurate methods would be the computation of the spectrum by a DFT for arbitrary frequencies, or by interpolation of the DFFT by convolution with *sinc* functions.

An accurate and efficient method for evaluating the measure H_1 consists in using the chirp z-transform (Oppenheim and Schaffer, 1978). The chirp z-transform is a technique for computing the values of the DFT at equal angles along a spiral in the complex z-plane. For the measure H_1, Equation (1), only the values around the unit circle are needed.

The derivation of the chirp z-transform starts with a change of variables in the formula of the DFT, and takes advantage of the possibility of evaluating the resulting expression by a convolution of two sequences.

M points, z_k, spaced at equal angles ω_0 along the unit circle, can be represented in the complex plane as:

$$z_k \;=\; W^{-k} \;=\; e^{-j\omega_0}, \text{for } k = 0, \ldots, M-1.$$

The definition of the DFT is:

$$X(z_k) \;=\; \sum_{n=0}^{N-1} x(n) W^{nk},$$

where the sequence of N samples $x(n)$ is modulated by the sequence W^{nk}, and then summed. The cost of evaluating the DFT by the above definition is proportional to $M \times N$.

Rewriting the above formula, and using the identity

$$nk = 1/2(n^2 \;+\; k^2 \;-(k-n)^2)$$

we obtain

$$X(z_k) \;=\; W^{k^2/2} \sum_{n=0}^{N-1} x(n) W^{-(k-n)^2/2},$$

where $x(n)$ is now convolved with $W^{-n^2/2}$. The convolution can be implemented with an FFT algorithm. The cost of the chirp z-transform is proportional to $(N + M - 1)log_2(N + M - 1)$.

Another estimator of the fundamental frequency of a sequence of harmonics, that I found useful is:

$$H_2(\tau_0) \;=\; |DFT^{-1}[log(F(\omega)]|.$$

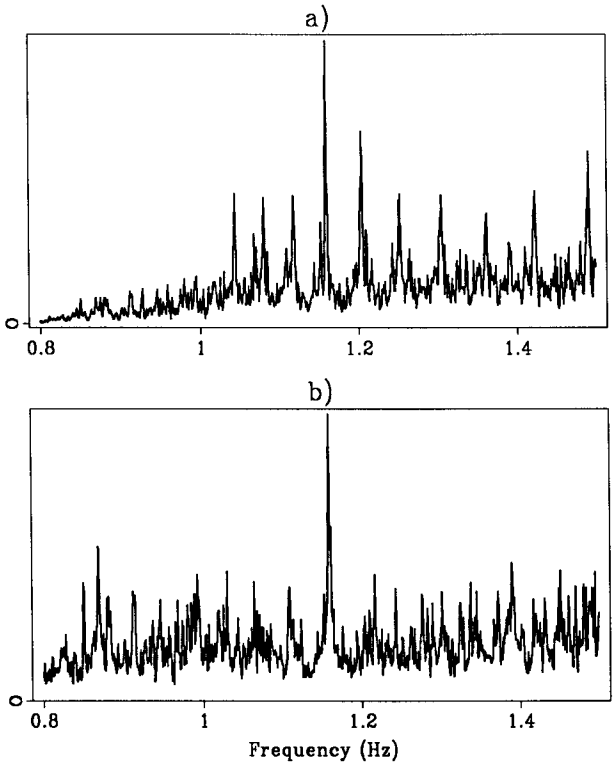

FIG. 12. Measure of the power of harmonic sequences. a) Vertical component of the accelerometer. b) Horizontal component of the accelerometer.

Without the logarithm, this measure H_2 is the absolute value of the autocorrelation. τ_0 is limited to a small interval around an initial guess in order to isolate one peak.

In principle, the autocorrelation could be used to estimate the fundamental frequency of the harmonic series. However, if the spectrum is not balanced, the autocorrelation will be dominated by a few sinusoids, and picking will be inaccurate. The logarithm balances the spectrum. Other ways to balance the spectrum would be to fit an autoregressive model with a small number of parameters to the data, for instance by applying Burg's algorithm (Marple, 1987), and then work with the residuals of the autoregressive model.

Examples

Figure 12 shows the measure H_1 computed using the chirp z-transform in the interval between 0.8 and 1.5Hz, on a grid with spacing 0.001Hz, for four traces recorded simultaneously. The interval of frequencies corresponds to 48 to 90 rotations per minute (rpm), while the rotation of the tool indicated on the drilling log is about 75 rpm. The value given by the drilling is only an indication, because (1) the measurement for the drilling log are for the accelerometers are not made at exactly the same time, and (2) the speed of rotation is measured at the top of the rig, which could be different from the speed of rotation of the drill-bit.

Two of the traces, Figures 12a and 12b, are the vertical and one of the horizontal components of the accelerometer. These traces show peaks at the same frequency equal to 1.16Hz. This frequency is the same on both records and could be the frequency of rotation of the tool.

The validity of the harmonic-sequence model, and of the hypothesis that the accelerometer record allows the estimation of the fundamental frequency of the drill-bit signal, should be tested further on data for which the drill-bit has been identified. The questions then would be how consistent are the moveout determined from the different harmonics, and whether it is possible to estimate the fundamental frequency from records other than the accelerometer.

ESTIMATION OF THE DRILL-BIT SIGNAL

Assuming that the drill-bit signal is radiated from an isotropic, compressional, point source, its wavefield can be characterized by delays across an array of receivers (at offset x, delay $\tau(x)$), and a wavelet $s(t)$.

In this section, I assume the delays $\tau(x)$ to be known and I review some basic methods for the estimation of $s(t)$ in the presence of uncorrelated or correlated noise. I assume further that the signal is narrow-band, possibly a component of a broad-band signal obtained by filtering with a bank of narrow-band filters. The delays across the array of the direct arrivals from the drill-bit can be obtained from velocity analysis of the drill-bit data, or from other data, such as surface seismic, or VSP. I also assume that amplitude amplitude variations with offset have been compensated.

Narrowband source, uncorrelated noise

The model for the data at a frequency ω is

$$D(x) \;=\; S + \; N(x),$$

where $D(x), S, \text{and} N(x)$ are the components of the FT at frequency ω and offset x, of the data $d(x,t)$, of the source wavelet $s(t)$, and of the noise $n(x,t)$.

The maximum-likelihood estimator of S, assuming zero-mean Gaussian noise, uncorrelated from offset to offset, is (Van Trees, 1964):

$$\hat{S} \;=\; \frac{1}{N} \sum_{x=1}^{x=N} D(x).$$

Narrowband source, correlated noise

Let the noise be correlated from offset to offset, with correlation matrix R_N, and inverse of the correlation matrix σ_N. Then, the maximum-likelihood estimator of

S is $\hat{S}$, found by minimizing the following objective function (Van Trees, 1964):

$$min \sum_{x,y} (D_x - \hat{S}) \sigma_{x,y} (\overline{D_y} - \overline{S}).$$

The difficulty in obtaining this estimator is that the correlation matrix of the noise is unknown.

Optimum linear filter

A slightly more general problem is obtained when the source wavelet $S(x)$ is allowed to vary with offset. I still consider signal and noise to be mutually uncorrelated, but both signal and noise are correlated from offset to offset. In the wavenumber domain, these correlations can be represented by the spectrum $S(k)$ for the signal, and $N(k)$ for the noise. Then, the optimum linear filter $H(k)$ in the wavenumber domain, or $h(x)$ in the offset domain, minimizes the mean-squared error (MSE)

$$E[(s(x) - h(x) * d(x))^2],$$

and is expressed as (Van Trees, 1964):

$$H(k) = \frac{S(k)}{S(k) + N(k)},$$

where $S(k) + N(k) = D(k)$, is the spectrum of the data.

Similarly to the maximum likelihood estimator, the optimum linear filter requires knowledge of the spectrum of the signal, or of the noise.

In cases, where the spectrum of the data shows two well-defined local maxima – one at low wavenumbers, and another one at high-wavenumbers – it might be possible to estimate the signal and noise spectra, respectively from the low-pass or high-pass filtered data.

Minimum variance estimator

Another approach to the estimation of the signal, follows the derivation of the minimum-variance spectral estimator (Marple, 1987), also known in array processing as the minimum-variance beamformer (Widrow and Stearns, 1985). The signal is estimated as a weighted average of the data,

$$\hat{S} = \sum_x w(x) D(x),$$

where $w(x)$ is interpreted as a window function. If the function $w(x)$ is constant, we obtain the optimal estimator for uncorrelated noise, and the amplitude of the window function in the wavenumber domain is a *sinc* function. With weights independent from the data, there is always the risk that peaks in the noise spectrum will coincide with peaks of the sidelobes of the window function, and thus degrade the

estimation. The data-adaptive determination of the window has the advantage of placing zeros in the spectrum of the weighting function, depending on the estimated spectrum of the noise.

The window function is determined by minimizing the following objective function with respect to $w(x)$:

$$\min|\sum_{\mathrm{x}} \mathrm{w(x)D(x)}|^2 = \mathrm{W^H R_D W}, \tag{2}$$

under the constraint

$$\sum_x w(x) = W^H \underline{\mathbf{1}} = 1.$$

The vector $\underline{\mathbf{1}}$, with components equal to unity, is introduced, because the signal is assumed to impinge with zero-delays at the array (after appropriate moveout correction).

An interpretation of the minimization problem (2) is that the minimum variance estimator minimizes the power in all directions of arrival except in the assumed "look" where the power is constrained to be constant.

The solutions for problem (2) are – for the weights:

$$\hat{w} \;=\; \frac{R_D^{-1}\underline{\mathbf{1}}}{\underline{\mathbf{1}}^H R_D^{-1}\underline{\mathbf{1}}},$$

and for the power of the signal:

$$|\hat{S}|^2 \;=\; \frac{1}{\underline{\mathbf{1}}^H R_d^{-1}\underline{\mathbf{1}}}.$$

This estimator performs well only when the signal and the noise are mutually uncorrelated in time. The next section illustrates this limitation with the example of two plane waves arriving at an array.

Example of signal cancellation for the minimum-variance estimator

The model for the data consists of two narrow-band plane waves; there is no receiver noise. In the time domain, after demodulation, the complex (analytic) representation of the data is:

$$D(x,t) \;=\; A(t) \;+\; B(t)e^{j\theta x}, \tag{3}$$

where $A(t)$ and $B(t)$ the source wavelets for the two plane waves. The correlation matrix of the data is

$$R_D \;=\; [\underline{\mathbf{1}}, U]^H \begin{bmatrix} 1 & \rho \\ \rho & 1 \end{bmatrix} [\underline{\mathbf{1}}, U]\,.$$

The vector U is the direction vector for the plane wave with wavelet $B(t)$; the components of U are $e^{j\theta x}$.

In equation (3), the power of each source is assumed unity,

$$\sum_t |A(t)|^2 \;=\; \sum_t |B(t)|^2 \;=\; 1,$$

and their cross correlation is ρ is:

$$\rho \;=\; \sum_t A(t) \times \bar{B}(t).$$

In the limit of a very narrow frequency band (as for a DFT), the time dependence in equation (4) is lost, and the two plane waves are fully correlated. In seismic applications, direct arrivals and reflected arrivals might be significantly correlated over a large band-width.

I derive now the expression for the output power of the minimum variance estimator in terms of the correlation between sources, following a method described in detail in a previous SEP report (Biondi and Kostov, 1988).

The eigenvalues of the correlation matrix R_D are $\lambda_1, \lambda_2, 0, \ldots, 0$, with

$$\lambda_1 \;=\; 1 \;+\rho, \text{ and } \lambda_2 \;=\; 1 \;-\rho.$$

The first two eigenvectors of the correlation matrix R_D are

$$E_1 \;=\; \frac{1+W}{\sqrt{2}},$$

and

$$E_2 \;=\; \frac{1-W}{\sqrt{2}}.$$

The generalized inverse of the correlation matrix R_D can be expressed now in terms of the eigenvalues and eigenvectors:

$$\mathbf{1}^H R_D^{-1} \mathbf{1} = \frac{1}{\lambda_1} |E_1{}^H \cdot \mathbf{1}|^2 \;+\; \frac{1}{\lambda_2} |E_2{}^H \cdot \mathbf{1}|^2 = \frac{1}{2}\left[\frac{1}{1+\rho} + \frac{1}{1-\rho}\right] = \frac{1}{1-\rho^2}.$$

The estimated power of the source is then:

$$|\hat{S}|^2 = 1 - \rho^2.$$

The power is correctly estimated as equal to 1 when the sources are uncorrelated, $\rho = 0$, but decreases to zero as the correlation between sources increases to full correlation, $\rho = 1$.

Further work

The above survey of methods for the estimation of the drill-bit wavelet should include a discussion of approaches to obtain the maximum-likelihood estimator for

narrow-band signals, and of methods that estimate broad-band sources without decomposing them into narrow-band components.

CONCLUSIONS

Work with the data from the OGS survey has allowed me to understand better the environment in which the data are recorded – how surface waves relate to the equipment on the platform, and how the drilling conditions influence the levels of signal and noise. The results of the spectral analysis show that there is some energy with moveout as expected from the drill-bit signal. Further processing could enhance that weak signal by using longer records in time, by coherent summation of gathers, and by introducing a model for the signal.

My recommendations for the next "VSP while-drilling" experiment are (1) to record with several seismic lines, (2) to try a "loop"-array to estimate the signal from the drill-bit, (3) to record for longer periods of time, and (4) to have a wider range of variation for the drilling parameters.

ACKNOWLEDGMENTS

I thank Professor Fabio Rocca and the Osservatorio Geofisico Sperimentale in Trieste for releasing the data to the SEP.

Discussions with C. Esmersoy, J. Haldorsen and D. Miller at Schlumberger-Doll Research, and with B. Biondi, F. Muir and F. Rocca at SEP, helped greatly to clarify the material presented in this report.

Part of the work on this report was done during a summer job with Schlumberger-Doll Research.

REFERENCES

Biondi, B., and Kostov, C., 1988, High-resolution velocity spectra using eigenstructure methods: SEP–**57**.

Dudgeon, D.E., Mersereau, R.M., 1984, Multidimensional signal processing: Prentice-Hall.

Hale, I.D., and Claerbout, J.F., 1983, Butterworth dip-filters: Geophysics, **48**, 1033-1038.

Kostov, C., and Zanzi, L., 1988, Analysis of drill-bit data: preliminary results: SEP–**57**.

Lutz, J., Raynaud, M., Gstalder, S., Quichaud, C., Raynal, J., Muckelroy, J.A., 1972, Instantaneous logging based on a dynamic theory of drilling: Journal of Petroleum Technology, JPT-3604.

Marple, S.L., 1987, Digital spectral analysis with applications: Prentice-Hall.

Osservatorio Geofisico Sperimentale (Trieste, Italy), 1988, Progetto Geobit, rapporto acqisizione dati: Osservatorio Geofisico Sperimentale.

Oppenheim, A., V., and Schafer, R.W., 1975, Digital signal processing: Prentice-Hall.

Van Trees, H.L., 1968, Detection, estimation, and modulation theory: J. Wiley & Sons.

Widrow, B., and Stearns, S.D., 1985, Adaptive signal processing: Prentice-Hall.